Optics Communications 394 (2017) 23–30

Contents lists available at ScienceDirect

Optics Communications

journal homepage: www.elsevier.com/locate/optcom

Sensitivity of sub-Planck structures of mesoscopically superposed coherent states to the thermal reservoirs induced decoherence

Parvendra Kumar[a,*], Ray-Kuang Lee[a,b]

[a] Institute of Photonics Technologies, National Tsing-Hua University, Hsinchu, Taiwan
[b] Department of Physics, National Tsing-Hua University, Hsinchu, Taiwan

ARTICLE INFO

Keywords:
Sub-Planck structures
Mesoscopically superposed coherent states
Dissipative thermal reservoir
Phase-damped thermal reservoir

ABSTRACT

We theoretically study the sensitivity of sub-Planck structures of mesoscopically superposed coherent states to the thermal reservoirs induced decoherence via dissipative and phase-damping processes, respectively. Under dissipative reservoir, we show that the *size* and *area* of the phase-space structures of cat and compass states do increase as the function of evolution-time, temperature of thermal reservoir, and cavity mode frequency. It is also shown that beyond the particular values of these parameters, the *size* and *area* of the phase-space structures remain no longer smaller than the limit set by the Heisenberg's uncertainty principle. Moreover we show that in contrast to the dissipative reservoir, the phase-space structures of the cat and compass states persist even in the infinitely-long evolution-time limit under phase-damped reservoir.

1. Introduction

Mesoscopically superposed coherent states have attracted a lot of attention as they show many unique nonclassical features [1–6]. The superposition of four specific coherent states or a so-called compass state reveals the interference structures in the Wigner phase-space description as noted by Zurek [7]. It contrast to the commonly held belief that the phase-space structures at the scales smaller than the limit set by the Heisenberg's uncertainty principle either do not exist or they do not have any observable consequence, the *area* of these interference structures is found to be much smaller than the limit set by the Heisenberg's uncertainty principle [7–10]. More importantly, it is demonstrated that such sub-Planck structures enhances the sensitivity of a quantum state to the external perturbations [7]. Later, it is demonstrated that a superposition of two specific coherent states or a so-called cat state also reveals the similar sub-Planck structures in the Wigner phase-space description [3,10]. These developments provide the new possibilities for carrying-out the Heisenberg-limited measurements. Indeed, it is recently proposed that the sub-Planck structures of mesoscopically superposed coherent states (MSCS) can be utilized for carrying-out the Heisenberg-limited measurement of a weak-force [10].

Several experimental and theoretical methods have been proposed to generate the MSCS. These includes the time evolution of a coherent state in the Kerr medium [11,12], fractional revival of molecular wave packets [13,14], and cavity quantum electrodynamics [15–17]. Particularly in cavity quantum electrodynamics, MSCS are generated by exploiting the dispersive interaction of high-quality cavities with the Rydberg atoms and superconducting qubits. However, it is important to note that generally MSCS are not completely isolated from their surrounding environment. Therefore the effects of environment, which always exists and can be modelled by the different types of thermal reservoirs, should be taken into account while exploiting the sub-Planck structures of MSCS. Indeed, the effects of thermal reservoirs on the evolution of coherence of MSCS and other quantum states are studied extensively [16–21]. However, so far the evolution of *size* or *area* of the sub-Planck structures of MSCS due to the thermal reservoirs is not studied explicitly despite the fact that it is the sub-Planck nature of these phase-space structures which is primarily responsible for Heisenberg-limited measurements.

In this paper, we investigate and clarify the role of thermal reservoirs induced decoherence on the phase-space structures of MSCS by analytically solving the appropriate master equations. To illustrate, we chose the cat and compass states as the two examples of MSCS. Related to our work, Kim and Bužek [19] have undertaken a theoretical study on the decay of the brightness of the sub-Planck structures and nonclassicality of the Schrödinger-cat states due to the loss of coherence via dissipative thermal reservoir only. In contrast to their work, the main focus of our work is to study the evolution of the *size* and *area* of the sub-Planck structures of cat and compass states due to the two different thermal reservoirs, including dissipative and phase-damped thermal reservoirs. We demonstrate explicitly that

* Corresponding author.
E-mail addresses: parvendra1986@gmail.com (P. Kumar), rklee@ee.nthu.edu.tw (R.-K. Lee).

http://dx.doi.org/10.1016/j.optcom.2017.02.066
Received 25 November 2016; Received in revised form 25 February 2017; Accepted 28 February 2017
Available online 07 March 2017
0030-4018/ © 2017 Elsevier B.V. All rights reserved.

under the influence of dissipative thermal reservoir not only the brightness of the sub-Planck structures of cat and compass states reduces but also their *size* and *area* become larger, simultaneously. It is also shown that beyond the particular values of evolution-time, temperature of thermal reservoir, and cavity mode frequency, the *size* and *area* of the phase-space structures remain no longer smaller than the limit set by the Heisenberg's uncertainty principle. Moreover, we show that unlike the dissipative reservoir, the Wigner functions of the cat and compass states exhibit the phase-space structures even in the infinitely-long evolution-time limit under phase-damped reservoir.

2. Theoretical formulation

The general superpositions of M coherent states can be written as: $|\varphi_n\rangle = N_n \sum_{k=1}^{M} |e^{i\varphi_k}\alpha\rangle$, $\varphi_k = 2\pi k/M$. The cat and compass states under study read as: $|\varphi_1\rangle = N_1(|\alpha\rangle + |-\alpha\rangle)$ and $|\varphi_2\rangle = N_2(|\alpha\rangle + |-\alpha\rangle + |i\alpha\rangle + |-i\alpha\rangle)$, respectively. We assume that the cat and compass states are stored in a superconducting cavity mode, which is coupled to the thermal reservoir of the cavity. In a cavity system, the thermal reservoir can be made of other freely propagating field modes coupled by diffraction on mirror defects, or electrons and Cooper pairs in the mirrors [22]. Here, $|\alpha\rangle$ and $|-\alpha\rangle$ represent the constituent coherent states of the cat state, while $|\alpha\rangle, |-\alpha\rangle, |i\alpha\rangle$, and $|-i\alpha\rangle$ represent the constituent coherent states of the compass state,N_1 and N_2 are the normalization constants. Under dissipative process, the time evolution of the cat and compass states can be described by the master equation [23]. It reads

$$\frac{d\rho^{1,2}(t)}{dt} = -i\omega_c[a^\dagger a, \rho^{1,2}] - \frac{\kappa(1+n_{th})}{2}(a^\dagger a\rho^{1,2} + \rho^{1,2}a^\dagger a - 2a\rho^{1,2}a^\dagger) - \frac{\kappa n_{th}}{2}(aa^\dagger\rho^{1,2} + \rho^{1,2}aa^\dagger - 2a^\dagger\rho^{1,2}a) \quad (1)$$

Here, $\rho^1(t)$ and $\rho^2(t)$ represent the time dependent density operators corresponding to the cat and compass states, respectively.ω_c,κ, and n_{th} represent the cavity mode frequency, cavity photon decay rate, and the mean number of thermal photons, respectively. Hereafter, we employ Eq. (1) in the interaction picture that's why the first term on the right side of Eq. (1) is neglected. We employ characteristic function approach for solving the Eq. (1). The symmetric- and normal-order characteristic functions are defined as [22]:

$$C_s^{\rho^{1,2}}(\lambda, \lambda^*, t) = Tr\left(\rho^{1,2}(t)e^{\lambda a^\dagger - \lambda^* a}\right), \quad (2a)$$

$$C_n^{\rho^{1,2}}(\lambda, \lambda^*, t) = Tr\left(\rho^{1,2}(t)e^{\lambda a^\dagger}e^{-\lambda^* a}\right) \quad (2b)$$

For a coherent state $|\alpha\rangle$, normal- and symmetric-order characteristic functions are related through the following relation [22]:

$$C_n^{|\alpha\rangle\langle\alpha|}(\lambda, \lambda^*, t) = e^{|\lambda|^2/2}C_s^{|\alpha\rangle\langle\alpha|}(\lambda, \lambda^*, t) \quad (3)$$

With the aid of Eq. (2b), Eq. (1) can be rewritten in the form of normal-order characteristic function. It reads

$$\frac{dC_n^{\rho^{1,2}}(\lambda, \lambda^*, t)}{dt} = -\frac{\kappa(1+n_{th})}{2}Tr\left((a^\dagger a\rho^{1,2} + \rho^{1,2}a^\dagger a - 2a\rho^{1,2}a^\dagger)e^{\lambda a^\dagger}e^{-\lambda^* a}\right) - \frac{\kappa n_{th}}{2}Tr\left((aa^\dagger\rho^{1,2} + \rho^{1,2}aa^\dagger - 2a^\dagger\rho^{1,2}a)e^{\lambda a^\dagger}e^{-\lambda^* a}\right) \quad (4)$$

Now, we consider the action of the differential operators $(\partial/\partial\lambda)$ and $(\partial/\partial\lambda^*)$ on the normal-order characteristic function to draw the correspondence between the derivatives of $C_n^{\rho^{1,2}}(\lambda, \lambda^*, t)$ and other normal-order characteristic functions of $a^\dagger a\rho^{1,2}$, $\rho^{1,2}a^\dagger a$,$a\rho^{1,2}a^\dagger$, $aa^\dagger\rho^{1,2}$, $\rho^{1,2}aa^\dagger$, and $a^\dagger\rho^{1,2}a$. After straightforward calculations, we obtain following relations:

$$C_n^{a^\dagger a\rho^{1,2}}(\lambda, \lambda^*, t) = C_n^{aa^\dagger\rho^{1,2}}(\lambda, \lambda^*, t) = \left(-\frac{\partial^2}{\partial\lambda^*\partial\lambda} + \lambda^*\frac{\partial}{\partial\lambda^*}\right)C_n^{\rho^{1,2}}(\lambda, \lambda^*, t), \quad (5a)$$

$$C_n^{\rho^{1,2}a^\dagger a}(\lambda, \lambda^*, t) = C_n^{\rho^{1,2}aa^\dagger}(\lambda, \lambda^*, t) = \left(-\frac{\partial^2}{\partial\lambda^*\partial\lambda} + \lambda\frac{\partial}{\partial\lambda}\right)C_n^{\rho^{1,2}}(\lambda, \lambda^*, t), \quad (5b)$$

$$C_n^{a\rho^{1,2}a^\dagger}(\lambda, \lambda^*, t) = \left(-\frac{\partial^2}{\partial\lambda^*\partial\lambda}\right)C_n^{\rho^{1,2}}(\lambda, \lambda^*, t), \quad (5c)$$

$$C_n^{a^\dagger\rho^{1,2}a}(\lambda, \lambda^*, t) = \left(-\frac{\partial^2}{\partial\lambda^*\partial\lambda} + \lambda\frac{\partial}{\partial\lambda} + \lambda^*\frac{\partial}{\partial\lambda^*} - |\lambda|^2\right)C_n^{\rho^{1,2}}(\lambda, \lambda^*, t) \quad (5d)$$

Using Eq. (5), we rewrite Eq. (4) in the form of normal-order characteristic functions. It reads

$$\frac{dC_n^{\rho^{1,2}}(\lambda, \lambda^*, t)}{dt} = -\kappa n_{th}|\lambda|^2 C_n^{\rho^{1,2}}(\lambda, \lambda^*, t) - \frac{\kappa}{2}\left(\lambda\frac{\partial C_n^{\rho^{1,2}}(\lambda, \lambda^*, t)}{\partial\lambda} + \lambda^*\frac{\partial C_n^{\rho^{1,2}}(\lambda, \lambda^*, t)}{\partial\lambda^*}\right) \quad (6)$$

Since the Wigner function of a quantum state can be calculated from its symmetric-order characteristic function. So now we convert Eq. (6) in the form of symmetric-order characteristic function by using Eq. (3). It reads

$$\frac{dC_s^{\rho^{1,2}}(\lambda, \lambda^*, t)}{dt} = -\kappa(n_{th} + 1/2)|\lambda|^2 C_n^{\rho^{1,2}}(\lambda, \lambda^*, t) - \frac{\kappa}{2}\left(\lambda\frac{\partial C_s^{\rho^{1,2}}(\lambda, \lambda^*, t)}{\partial\lambda} + \lambda^*\frac{\partial C_s^{\rho^{1,2}}(\lambda, \lambda^*, t)}{\partial\lambda^*}\right) \quad (7)$$

The density operator corresponding to the cat state, $|\varphi_1\rangle$, is given by

$$\rho_s^1(t=0) = |\varphi_1\rangle\langle\varphi_1| = |N_1|^2(|\alpha\rangle\langle\alpha| + |-\alpha\rangle\langle-\alpha| + |\alpha\rangle\langle-\alpha| + |-\alpha\rangle\langle\alpha|) \quad (8)$$

Similarly, the density operator corresponding to the compass state can be calculated as:$\rho_s^2(t=0) = |\varphi_2\rangle\langle\varphi_2|$. The normalization constants are given as: $|N_1|^2 = 1/2\left(1 + e^{-2|\alpha|^2}\right)$ and $|N_2|^2 = 1/4\left(1 + e^{-2|\alpha|^2} + e^{-|\alpha|^2(1-i)} + e^{-|\alpha|^2(1+i)}\right)$. With the aid of Eq. (2a), the initial symmetric-order characteristic function corresponding to a general density operator $|\alpha\rangle\langle\beta|$ is given by

$$C_s^{|\alpha\rangle\langle\beta|}(\lambda, \lambda^*, t=0) = e^{-\frac{(|\alpha|^2+|\alpha|^2+|\beta|^2-2\alpha\beta^*)}{2} + \beta^*\lambda - \alpha\lambda^*} \quad (9)$$

For this symmetric-order characteristic function, we seek a solution of Eq. (7) in the form:

$$C_s^{|\alpha\rangle\langle\beta|}(\lambda, \lambda^*, t) = e^{-\frac{(|\alpha|^2+|\beta|^2-2\alpha\beta^*)}{2}}e^{(a(t)|\lambda|^2 + b(t)\lambda + c(t)\lambda^*)} \quad (10)$$

subjected to the initial conditions,$a(0) = -1/2$, $b(0) = \beta^*$, and $c(0) = -\alpha$. After substituting Eq. (10) in Eq. (7) and employing the initial conditions, the solution of Eq. (7) for a general density operator $|\alpha\rangle\langle\beta|$ is given by

$$C_s^{|\alpha\rangle\langle\beta|}(\lambda, \lambda^*, t) = e^{-\frac{(|\alpha|^2+|\beta|^2-2\alpha\beta^*)}{2}}e^{-\left(\frac{|\lambda|^2}{2} + |\lambda|^2 n_{th}(1-e^{-\kappa t}) - \beta^*\lambda e^{-\kappa t/2} + \alpha\lambda^* e^{-\kappa t/2}\right)} \quad (11)$$

With the aid of Eq. (11), the symmetric-order characteristic function of the cat (compass) state can be obtained by summing-up all the symmetric-order characteristic functions corresponding to each individual density operators of the cat (compass) state. The Wigner functions of the cat and compass states can be calculated as [19]:

$$W^{|\varphi_1\rangle,|\varphi_2\rangle}(\gamma,\gamma^*,t)=\int_{-\infty}^{+\infty}d^2\lambda C_s^{\rho^{1,2}}(\lambda,\lambda^*,t)e^{\gamma\lambda^*-\gamma^*\lambda} \tag{12}$$

After substituting the value of time dependent symmetric-order characteristic function corresponding to the cat sate in Eq. (12), the Wigner function of the cat state is given by

$$W^{|\varphi_1\rangle}(\gamma,\gamma^*,t)=\frac{|N_1|^2}{\pi D(t)}\left(e^{-\frac{1}{D(t)}|\gamma-\alpha_t|^2}+e^{-\frac{1}{D(t)}|\gamma+\alpha_t|^2}+2e^{-\frac{1}{D(t)}|\gamma|^2}e^{-|\alpha|^2(2-E(t))}\cos\left(\frac{2\alpha_t\gamma''}{D(t)}\right)\right) \tag{13}$$

Here, $D(t)=1/2+n_{th}(1-e^{-\kappa t})$, $E(t)=e^{-\kappa t}/D(t)$,$n_{th}=(e^{h\omega_c/KT}-1)^{-1}$, $\alpha_t=\alpha e^{-\kappa t/2}$ and $\gamma=\gamma'+i\gamma''$. Where, α, h, K and T represent the amplitude of the coherent state, Planck constant, Boltzmann constant, and temperature of thermal reservoir, respectively. The term $D(t)$ represents the dispersion of coherent states due to the flow of fluctuation energy from the thermal reservoir into the cavity mode. The first two-terms on the right-hand side of Eq. (13) represent the Wigner functions of the individual coherent states of the cat state, while the last cosine term represents the quantum interference between these two coherent states. This interference term is of the great interest, since it leads to the formation of phase-space structures at the scales much smaller ($<<\hbar/2$) than the limit set by the Heisenberg's uncertainty principle ($\geq\hbar/2$) along γ'' direction. The *size* ($\Delta\gamma''$) of these phase-space structures is obtained from the condition at which the cosine term in Eq. (13) vanishes. It reads

$$\Delta\gamma''=\frac{\pi D(t)}{2\alpha_t} \tag{14}$$

After following the procedure similar to that for the cat state, the Wigner function of the compass state is given by

$$W^{|\varphi_2\rangle}(\gamma,\gamma^*,t)=\frac{|N_2|^2}{\pi D(t)}\left(\begin{array}{l}e^{-\frac{1}{D(t)}|\gamma-\alpha_t|^2}+e^{-\frac{1}{D(t)}|\gamma+\alpha_t|^2}+e^{-\frac{1}{D(t)}|\gamma-i\alpha_t|^2}+e^{-\frac{1}{D(t)}|\gamma+i\alpha_t|^2}\\+2e^{-\frac{1}{D(t)}|\gamma|^2}e^{-|\alpha|^2(2-E(t))}\left\{\cos\left(\frac{2\alpha_t\gamma''}{D(t)}\right)\right.\\\left.+\cos\left(\frac{2\alpha_t\gamma'}{D(t)}\right)\right\}+2e^{-\frac{1}{D(t)}|\gamma|^2}e^{-|\alpha|^2(1-i(1-E(t)))}\\\left\{\cosh\left(\frac{\alpha_t}{D(t)}((\gamma'+\gamma'')-i(\gamma'+\gamma''))\right)\right.\\\left.+\cosh\left(\frac{\alpha_t}{D(t)}((\gamma'-\gamma'')-i(\gamma'-\gamma''))\right)\right\}+2e^{-\frac{1}{D(t)}|\gamma|^2}\\e^{-|\alpha|^2(1+i(1-E(t)))}\\\times\left\{\cosh\left(\frac{\alpha_t}{D(t)}((\gamma'+\gamma'')+i(\gamma'+\gamma''))\right)\right.\\\left.+\cosh\left(\frac{\alpha_t}{D(t)}((\gamma'-\gamma'')+i(\gamma'-\gamma''))\right)\right\}\end{array}\right) \tag{15}$$

The first four-terms on the right-hand side of Eq. (15) represent the Wigner functions of the individual coherent states of the compass state, while the fifth cosine term is of the greatest importance since it leads to the formation of phase-space structures at the scales much smaller ($<<\hbar/2$) than the limit set by the Heisenberg's uncertainty principle ($\geq\hbar/2$) along the arbitrary direction in the central region of phase-space. The other remaining cosine-hyperbolic terms reveal the oblique interference patterns in phase-space. The *area* (A) of the phase-space structures corresponding to the fifth term of Eq. (15) is obtained from the condition at which this term vanishes. It reads

$$A=\frac{\pi^2D^2(t)}{2\alpha_t^2} \tag{16}$$

Under phase-damping process, the time evolution of the cat and compass states can be described by the master equation [23–26]. In the interaction picture, it reads

$$\frac{d\rho^{1,2}}{dt}=-\kappa'(a^\dagger aa^\dagger a\rho^{1,2}+\rho^{1,2}a^\dagger aa^\dagger a-2a^\dagger a\rho^{1,2}a^\dagger a) \tag{17}$$

where $\kappa'=\frac{\kappa(1+2n_{th})}{2}$. In general, the phase-damping of a quantum system takes place due to elastic scattering of the thermal reservoir photons through the quantum system itself. The solution of Eq. (17) can be written in coherent states basis. It reads

$$\rho^{1,2}(t)=\int_{-\infty}^{+\infty}\int_{-\infty}^{+\infty}\frac{d^2p}{\pi}\frac{d^2q}{\pi}\rho_{pq}^{1,2}(t)|p\rangle\langle q| \tag{18}$$

The density matrix element $\rho_{pq}^{1,2}(t)$ is calculated by putting Eq. (18) into Eq. (17). It reads

$$\rho_{pq}^{1,2}(t)=\rho_{pq}^{1,2}(t=0)e^{-\kappa' t\left(|p|^2-|q|^2\right)^2} \tag{19}$$

From Eqs. (18) and (19), the solution of Eq. (17) reads

$$\rho^{1,2}(t)=\int_{-\infty}^{+\infty}\int_{-\infty}^{+\infty}\frac{d^2p}{\pi}\frac{d^2q}{\pi}\rho_{pq}^{1,2}(t=0)e^{-\kappa' t\left(|p|^2-|q|^2\right)^2}|p\rangle\langle q| \tag{20}$$

It is easy to recognize that in the long evolution-time limit ($\kappa' t\to\infty$) only diagonal elements,$\rho_{pp}^{1,2}$, can survive under phase-damping process. Thus in the long evolution-time limit ($\kappa' t\to\infty$), the solution of Eq. (17) can be written as

$$\rho^{1,2}(\kappa' t\to\infty)=\int_{-\infty}^{+\infty}\frac{d^2p}{\pi}\rho_{pp}^{1,2}(t=0)|p\rangle\langle p| \tag{21}$$

The Wigner functions of the cat and compass states under phase-damping process, in the long evolution-time limit ($\kappa' t\to\infty$), can be calculated as [16]:

$$W^{|\varphi_1\rangle,|\varphi_2\rangle}(\gamma,\gamma^*,t\to\infty)=\frac{2e^{2|\gamma|^2}}{\pi^2}\int_{-\infty}^{+\infty}d^2\beta\langle-\beta|\rho^{1,2}(\kappa' t\to\infty)|\beta\rangle e^{-2(\beta\gamma^*-\beta^*\gamma)} \tag{22}$$

The Wigner function of the cat state is obtained by calculating $\rho^1(\kappa' t\to\infty)$ through Eq. (21). It reads

$$W^{|\varphi_1\rangle}(\gamma,\gamma^*,t)=\frac{2|N_1|^2}{3\pi}\left(e^{-\frac{2}{3}|\gamma-\alpha|^2}+e^{-\frac{2}{3}|\gamma+\alpha|^2}+2e^{-\frac{2}{3}|\gamma|^2}e^{-\frac{4}{3}|\alpha|^2}\cos\left(\frac{4\alpha\gamma''}{3}\right)\right) \tag{23}$$

Similar to the Eq. (13), the first two terms on the right-hand side of Eq. (23) represent the Wigner functions of the individual coherent states, while the last cosine term represents their interference. The *size* ($\Delta\gamma''$) of phase-space structures corresponding to this cosine term is given by

$$\Delta\gamma''=\frac{3\pi}{4\alpha} \tag{24}$$

The Wigner function of the compass state is obtained by calculating $\rho^2(\kappa' t\to\infty)$ through Eq. (22). It reads

$$W^{|\varphi_2\rangle}(\gamma,\gamma^*,t)=\frac{2\,|N_2|^2}{3\pi}\left(\begin{array}{l} e^{-\frac{2}{3}|\gamma-\alpha|^2}+e^{-\frac{2}{3}|\gamma+\alpha|^2}+e^{-\frac{2}{3}|\gamma-i\alpha|^2}+e^{-\frac{2}{3}|\gamma+i\alpha|^2} \\ +2e^{-\frac{2}{3}|\gamma|^2}e^{-\frac{4}{3}|\alpha|^2}\times\{\cos(\frac{4\alpha\gamma''}{3}) \\ +\cos(\frac{4\alpha\gamma'}{3})\}+2e^{-\frac{2}{3}|\gamma|^2}e^{-\frac{4}{3}|\alpha|^2(1+i/3)} \\ \{\cosh(\frac{2\alpha}{3}((\gamma'+\gamma'')-i(\gamma'+\gamma'')) \\ +\cosh(\frac{2\alpha}{3}((\gamma'-\gamma'')-i(\gamma'-\gamma'')))\} \\ +2e^{-\frac{2}{3}|\gamma|^2}e^{-\frac{4}{3}|\alpha|^2(1+i/3)} \\ \times\{\cosh(\frac{2\alpha}{3}((\gamma'+\gamma'')+i(\gamma'+\gamma'')) \\ +\cosh(\frac{2\alpha}{3}((\gamma'-\gamma'')+i(\gamma'-\gamma'')))\} \end{array}\right) \tag{25}$$

The first four-terms on the right-hand side of Eq. (25) represent the Wigner functions of the individual coherent states; while the fifth term associated with the cosine functions represent their interference pattern. The other remaining cosine-hyperbolic terms represent the interference between two individual coherent states. The *area* (A) of the phase-space structures corresponding to fifth cosine term is given by

$$A=\frac{9\pi^2}{8\alpha^2} \tag{26}$$

It is easy to understand from Eqs. (14) and (24) that the *size* of sub-Planck structures of cat state is inversely proportional to the phase-space distance (2α) between its constituent coherent states, $|\alpha\rangle$ and $|-\alpha\rangle$. Therefore the defined notions of *size* can be generalized to other superposed coherent states wherein the sub-Planck structures arise due to interference between two arbitrary coherent states only by putting the phase-space distance of the concerned coherent states in place of 2α. Regarding the generalized notion of *area* of 2-D sub-Planck structures, we find that the shapes (square, circular or triangular, etc.) of these sub-Planck structures get changed depending upon the number of superposed coherent states participating in the formation of these interference patterns. Therefore the separate definitions of *area,* for the particular sets of superimposed coherent states, should be more appropriate for the quantitative analysis of their evolution under dissipative and phase-damped reservoirs.

3. Results and discussions

We now study the time evolution of the Wigner functions of the cat and compass states for the realistic values of involved parameters. The typical value of cavity mode frequency (ω_c) is considered to be 48.18 GHz [17]. In Fig. 1, we show the Wigner functions of the cat state for the different values of coherent state amplitude (α), evolution-time (κt), and temperature of thermal reservoir (T). In Fig. 1(a), the Wigner function of the cat state for $\alpha=3$, $\kappa t=0$, and $T=0\,mK$ is shown. The Wigner function of an individual coherent state (right- and left-hand side) and their interference patterns comprising the phase-space structures in the central region can be observed.

Next in Fig. 1(b), we present the Wigner function of the cat state with the same value of α but for the non-zero values of evolution-time and temperature of thermal reservoir ($\kappa t=0.02$, $T=10\,mK$). It can be observed from Fig. 1(b) that the brightness of the Wigner functions of individual coherent states and phase-space structures gets reduced. This is due to the decay and dispersion of the amplitude of coherent states under non-zero values of evolution-time ($\kappa t=0.02$) and temperature of thermal reservoir ($T=10\,mK$) (See Eq. (13)), respectively. In Fig. 1(c), we show the Wigner function of the cat state for $\alpha=5$, $\kappa t=0$, and $T=0\,mK$. It can be observed that the *size* ($\Delta\gamma''$) of phase-space structures is smaller compared to those in Fig. 1(a), because the *size* ($\Delta\gamma''$) of the phase-space structures is inversely proportional to α_t (See Eq. (14)). In Fig. 1(d), we show the Wigner function of the cat state for $\alpha=5$, $\kappa t=0.02$, and $T=10\,mK$. It can be observed from Fig. 1(d) that for the increased value of α, the brightness of phase-space structures gets reduced sharply compared to those in Fig. 1(b).

In Fig. 2(a), we show the Wigner function of the compass state for $\alpha=3$, $\kappa t=0$, and $T=0\,mK$. The Wigner functions of individual coherent states and their interference patterns comprising the phase-space structures, in the central region, can be observed. It is important to note that the phase-space structures of the compass state are formed along both the directions (γ' and γ'') in contrast to those of the cat state. The additional oblique phase-space structures appear due to the interference between two individual coherent states. In Fig. 2(b), we show the Wigner function of the compass state for the non-zero values of evolution-time ($\kappa t=0.02$) and temperature of thermal reservoir ($T=10\,mK$). Similar to Fig. 1(b), the brightness of the Wigner functions of individual coherent states and their interference patterns gets reduced under the non-zero values of evolution-time ($\kappa t=0.02$) and temperature of thermal reservoir ($T=10\,mK$). It can be observed from Fig. 2(c) that for the increased value of α, the *area* (A) of the phase-space structures is smaller compared to those in Fig. 2(a), because the *area* (A) of phase-space structures is found to be inversely proportional to α_t^2 (See Eq. (16)).

Similar to the Fig. 1(d), the brightness of phase-space structures gets reduced sharply for the increased value of α under non-zero values evolution-time ($\kappa t=0.02$) and temperature of thermal reservoir ($T=10\,mK$) as can be observed in Fig. 2(d). It can be understood from Figs. 1(d) and (d) that the brightness of phase-space structures of the cat and compass sates gets reduced quickly for the increased values of α under the non-zero values of evolution-time (κt) and temperature of thermal reservoir (T). Therefore, hereafter we focus on the dissipative process induced evolution of phase-space structures of the cat and compass states with $\alpha=3$.

In Fig. 3, we focus only on the phase-space structures that appear in central phase-space region of the Wigner functions of the cat and compass states. It can be observed by comparing Figs. 3(a) and (b) that the *size* ($\Delta\gamma''$) of the phase-space structures is larger for the non-zero values of evolution-time ($\kappa t=0.02$) and temperature of thermal reservoir ($T=2\,K$). Similarly, the *Area* (A) of the phase-space structures is larger for the non-zero values of evolution-time ($\kappa t=0.02$) and temperature of thermal reservoir ($T=2\,K$) as can be observed by comparing Figs. 3(c) and (d). The size (area) of the phase-space structures of cat (compass) state increases because the phase-space separation between the constituent coherent states decreases due to their decay and dispersion under dissipative process.

For more quantitative analysis, in Fig. 4, we show the evolution of the *size* (*area*) of the phase-space structures of the cat (compass) state as a function of evolution-time (κt) under the different values of temperature of thermal reservoir (T). It can be observed from Figs. 4(a) and (b) that the *size* (*area*) of the phase-space structures of cat (compass) state does increase rapidly for the non-zero values of temperature of thermal reservoir ($T\neq 0\,K$) compared to that of zero temperature reservoir (T=0 K). Therefore the temperature of thermal reservoir plays a substantial role in the evolution of phase-space structures. Figs. 4(a) and (b) also reveal that beyond the particular values of evolution-time ($\kappa t>0.04$) and temperature of thermal reservoir ($T=4K$), the *size* ($\Delta\gamma''$) and area (A) of the phase-space structures of the cat and compass states remain no longer smaller ($\Delta\gamma''<1/2$, $A<1/2(\hbar=1)$) than the limit set by the Heisenberg's uncertainty principle. We find that for the typical values of cavity decay rate ($\kappa=7.2KHz(\kappa^{-1}=0.13ms)$) and temperature of thermal reservoir ($T=4K$) [6,27,28], the *size* ($\Delta\gamma''$) and *area* (A) of phase-space structures becomes greater than 0.5 ($\Delta\gamma''>1/2, A>1/2$) for $t>0.0055\,ms$. Therefore a quantum measurement which aims to exploit the sub-Planck structures to achieve the Heisenberg-limited sensitivity should be completed within the time-scale of at least two-orders of magnitude shorter than the cavity decay time (κ^{-1}). It is also clear from Figs. 4(a) and (b) that the *size* of sub-Planck structures is less sensitive to the dissipative reservoir compared to that of *area* as the former increases slowly with respect to the time-evolution.

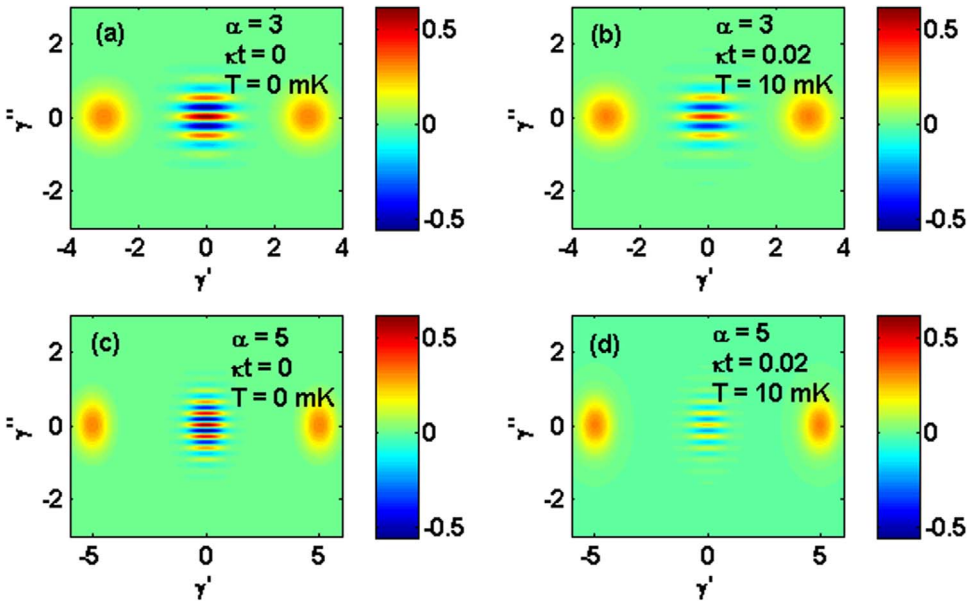

Fig. 1. Evolution of the Wigner functions of the cat state for the different values of coherent state amplitude (α), evolution-time (κt), and temperature of thermal reservoir (T). (a) $\alpha = 3$, $\kappa t = 0$, and $T = 0\ mK$, (b) $\alpha = 3$, $\kappa t = 0.02$, and $T = 10\ mK$, (c) $\alpha = 5$, $\kappa t = 0$, and $T = 0\ mK$, and (d) $\alpha = 5$, $\kappa t = 0.02$, and $T = 10\ mK$.

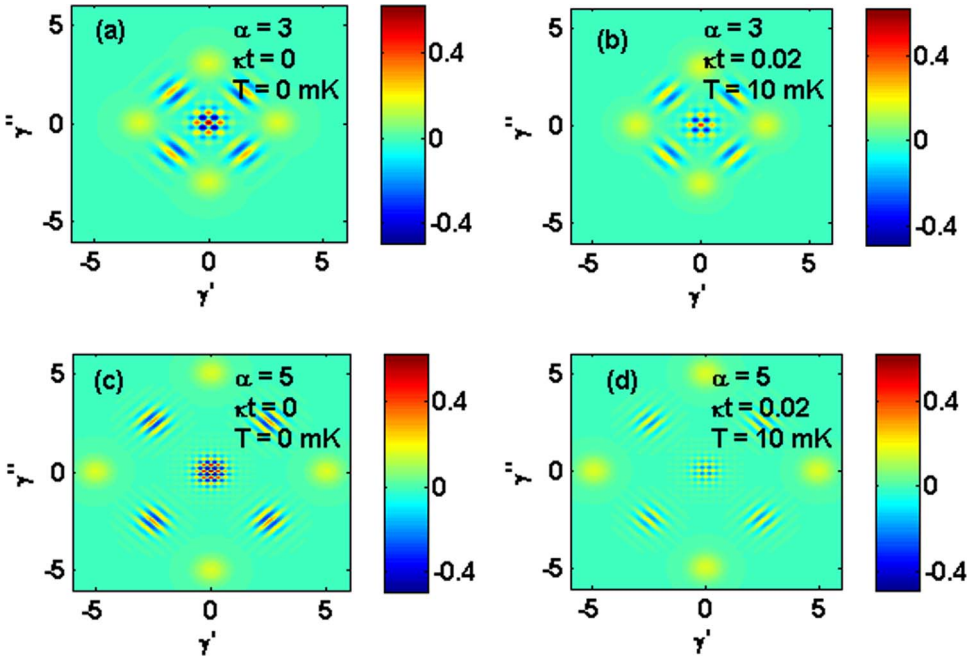

Fig. 2. Evolution of the Wigner functions of the compass state for the different values of coherent state amplitude (α), evolution-time (κt), and temperature of thermal reservoir (T). (a) $\alpha = 3$, $\kappa t = 0$, and $T = 0\ mK$, (b) $\alpha = 3$, $\kappa t = 0.02$, and $T = 10\ mK$, (c) $\alpha = 5$, $\kappa t = 0$, and $T = 0\ mK$, and (d) $\alpha = 5$, $\kappa t = 0.02$, and $T = 10\ mK$.

In all the results presented so far we employ the constant value of cavity mode frequency ($\omega_c = 48.18\ GHz$). However, in the different experimental designs the value of cavity frequency can be different. Therefore, in Fig. 5, we analyze the evolution of *size* (*area*) of the phase-space structures of the cat (compass) state as the function of cavity mode frequency (ω_c) and temperature of thermal reservoir (T) for a fixed value of the evolution-time ($\kappa t = 0.02$). It can be observed from Figs. 5(a) and (b) that the *size* (*area*) of the phase-space structures of the cat (compass) state does increase as the function of cavity mode frequency (ω_c) and temperature of thermal reservoir (T). We find that for the cavity mode frequencies,$\omega_c < 16.4(21.8)GHz$, and thermal-reservoir-temperature,$T = 3(4)K$, the *size* ($\Delta\gamma''$) of the phase-space structures of the cat state remain no longer smaller ($\Delta\gamma'' < 1/2(\hbar = 1)$) than the limit set by the Heisenberg's uncertainty principle as can be observed from Fig. 5(a). Similarly, the *area* (A) of the phase-space structures of the compass state remain no longer smaller ($A < 1/2(\hbar = 1)$) than the limit set by the Heisenberg's uncertainty principle for the cavity mode frequencies, $\omega_c < 16.7(22.3)GHz$, and thermal-reservoir-temperature, $T = 3(4)K$, as can be observed from Fig. 5(b).

It can be understood from Figs. 1 and 2 that the phase space structures shall vanish in the long evolution-time limit ($\kappa' t \to \infty$) under dissipative processes. However, in Fig. 6, we show the Wigner functions of the cat state under long evolution-time limit ($\kappa' t \to \infty$) to compare these results with their counterparts under phase-damping process. In Fig. 6, we show the Wigner function of a cat state at two different temperatures.

It can be observed from Fig. 6(a) that under long evolution-time

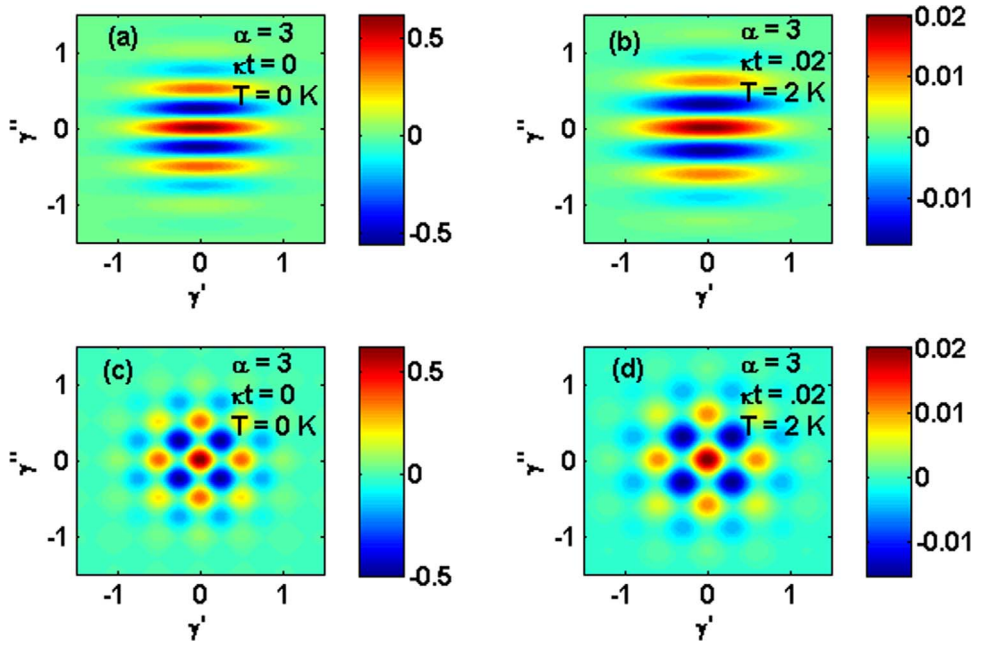

Fig. 3. Central phase-space structures in the Wigner functions of the cat (a, b) and compass (c, d) states for the different values of evolution-time (κt) and temperature of thermal reservoir (T). (a) $\alpha = 3$, $\kappa t = 0$, and $T = 0\,K$, (b) $\alpha = 3$, $\kappa t = 0.02$, and $T = 2\,K$, (c) $\alpha = 3$, $\kappa t = 0$, and $T = 0\,K$, and (d) $\alpha = 3$, $\kappa t = 0.02$, and $T = 2\,K$.

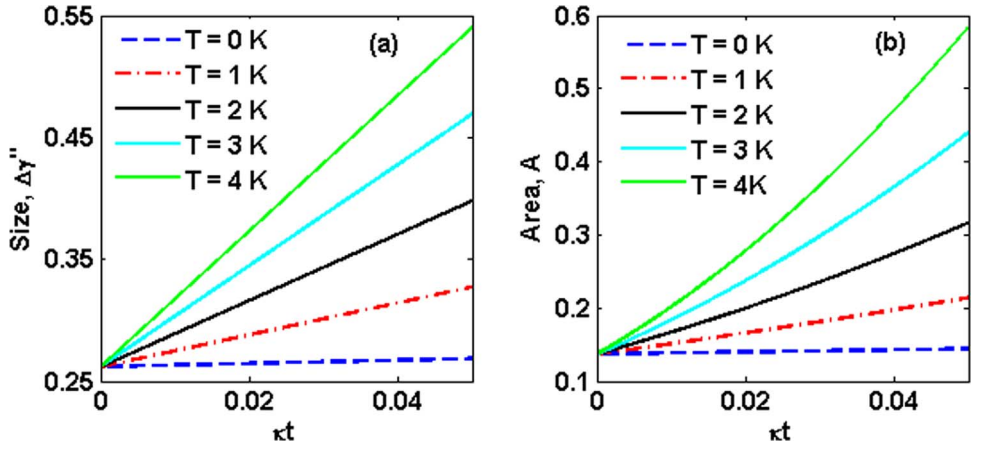

Fig. 4. Evolution of the *size* ($\Delta\gamma''$) and *area* (A) of the phase-space structures of the cat (a) and compass (b) state as a function of evolution-time (κt) under the different values of temperature of thermal reservoir (T) and $\alpha = 3$.

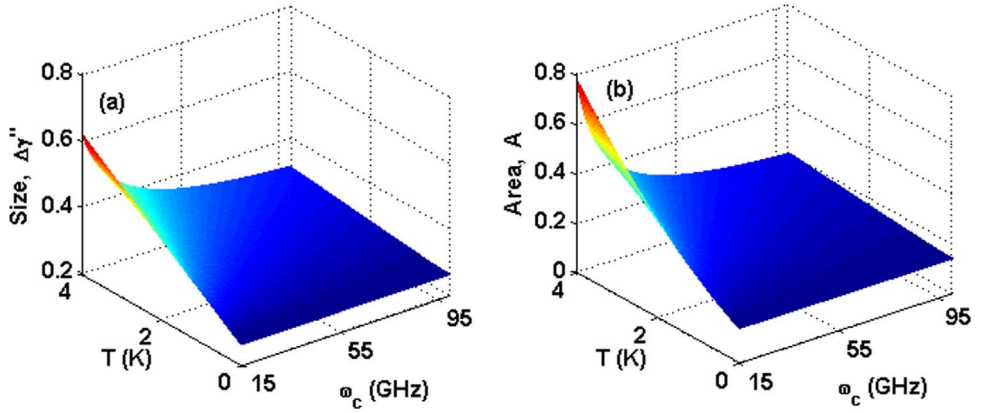

Fig. 5. The evolution of the size ($\Delta\gamma''$) and area (A) of the phase-space structures of the cat (a) and compass (b) states as a function of thermal-reservoir-temperature (T) and cavity mode frequency (ω_c) for a fixed value of evolution-time ($\kappa t = 0.02$) and $\alpha = 3$.

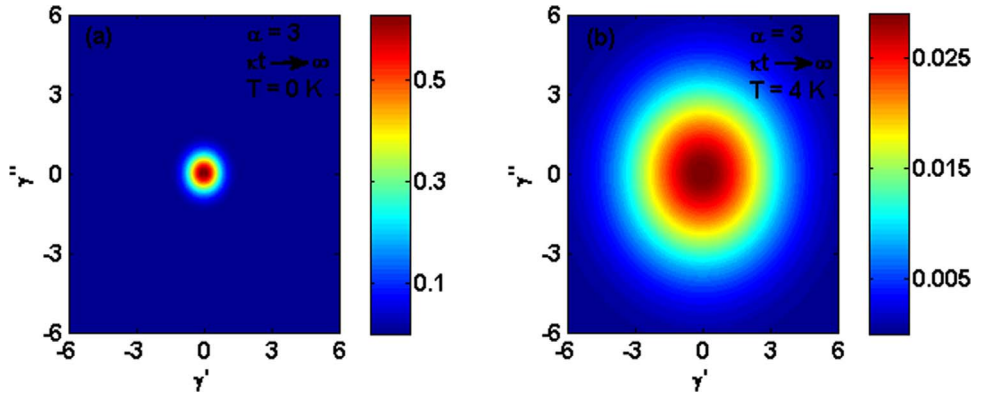

Fig. 6. The Wigner functions of the cat state for two different values of temperature of thermal reservoir (T) under long evolution-time limit ($\kappa' t \to \infty$). (a) $\alpha = 3$, $\kappa' t \to \infty$, $T = 0K$, and (b) $\alpha = 3$, $\kappa' t \to \infty$, $T = 4K$.

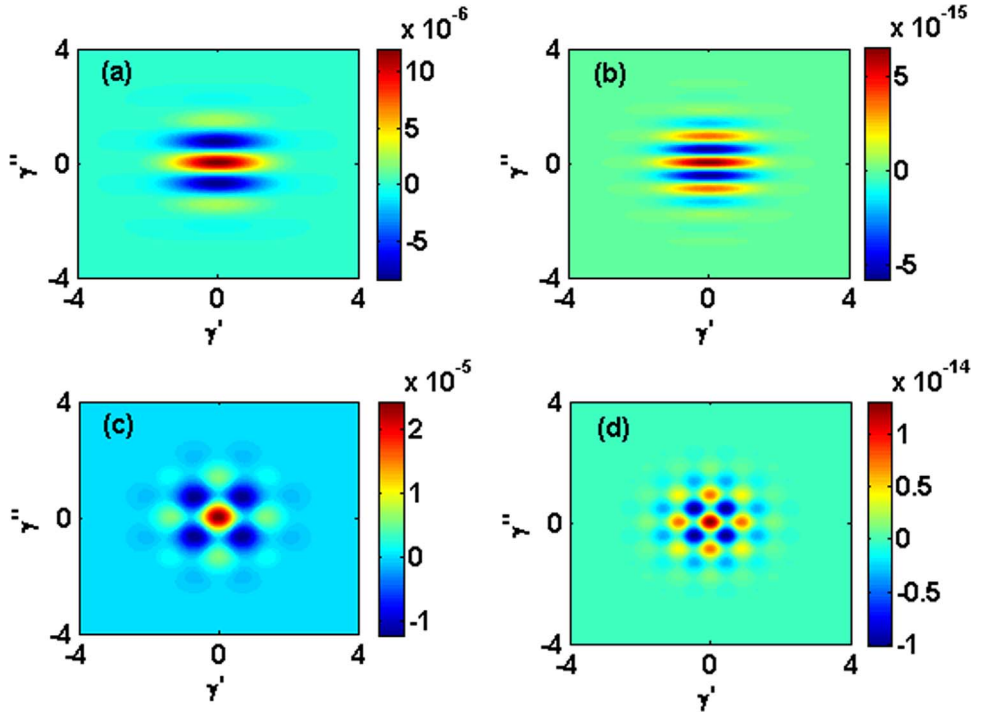

Fig. 7. Central phase-space structures in the Wigner functions of the cat (a, b) and compass (c, d) states under phase-damping process in long evolution-time limit ($\kappa' t \to \infty$). $\alpha = 3$ in (a) and (c), $\alpha = 5$ in (b) and (d).

limit ($\kappa' t \to \infty$) and zero-temperature thermal reservoir ($T = 0\ K$), the Wigner function of the cat state is transformed into the Wigner function that of a vacuum state due to the loss of cavity photons to the thermal reservoir. However for the non-zero value of temperature of thermal reservoir ($T = 4\ K$) in Fig. 6(b), the Wigner function of the cat state is transformed into the Wigner function that of a thermal state due to the loss of cavity photons to the thermal reservoir and flow of thermal fluctuation energy from the reservoir into the cavity mode, simultaneously. Under long evolution-time limit ($\kappa' t \to \infty$), we find that the Wigner function of the compass state is also transformed into the Wigner function that of a vacuum and thermal state for $T = 0\ K$ and $T = 4\ K$, respectively.

In Fig. 7, we now show the phase-space structures that appear in central phase-space region of the Wigner functions of the cat and compass states under phase-damping process in the long evolution-time limit ($\kappa' t \to \infty$). In contrast to the dissipative process induced decoherence, the phase-space structures of the cat and compass sates do survive under phase-damping induced decoherence even in the long evolution-time limit ($\kappa' t \to \infty$) as can be observed by comparing Figs. 6 and 7. However, the magnitude of the phase-space structures gets reduced due to the partial loss of coherence under phase-damping process, particularly for the larger value of α (See third term in Eq. (23) and fifth term in Eq. (25)).

It can also be observed from Figs. 7(a) and (b) that the *size* ($\Delta\gamma''$) of phase-space structures of the cat state is smaller for the larger value of α, because the *size* ($\Delta\gamma''$) of phase-space structures is inversely proportional to α (See Eq. (24)). Similarly the *area* (A) of phase-space structures of compass state is smaller for the larger value of α, because the *area* (A) of phase-space structures is inversely proportional to α^2 (See Eq. (26)). This can be observed from Figs. 7(c) and (d).

Finally in Fig. 8, we show the evolution of the *size* ($\Delta\gamma''$) and *area* (A) of the phase-space structures of cat and compass states under phase-damping process in the long evolution-time limit ($\kappa' t \to \infty$) as a function of coherent state amplitude (α). It can be observed that for the increased value of coherent state amplitude (α), the *size* ($\Delta\gamma''$) and *area* (A) of the phase-space structures of cat and compass states becomes smaller than 0.5 ($\Delta\gamma'' < 1/2, A < 1/2$). Therefore under phase-damping process, the sub-Planck nature of the phase-space structures of cat and

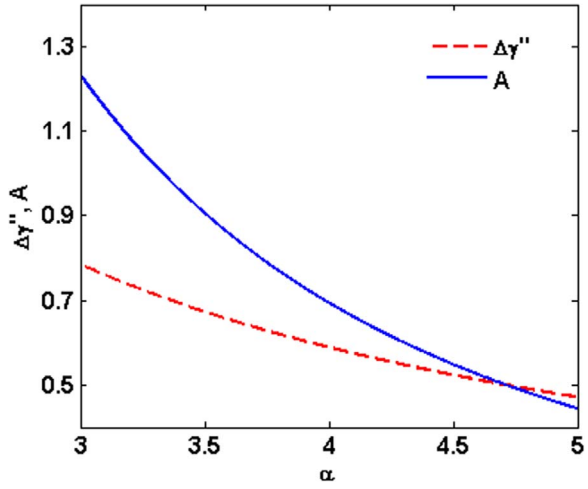

Fig. 8. The evolution of the *size* ($\Delta\gamma''$) and *area* (A) of the phase-space structures of cat (dashed-red line) and compass (solid-blue line) states under phase-damping process in the long evolution-time limit ($\kappa' t \to \infty$) as a function of coherent state amplitude (α). (For interpretation of the references to color in this figure legend, the reader is referred to the web version of this article).

compass states can persist even in the long evolution-time limit ($\kappa' t \to \infty$), but at the expense of reduced magnitudes of their Wigner functions (see Fig. 7).

4. Conclusions

In conclusion, we have theoretically investigated the sensitivity of the phase-space structures of cat and compass states to the thermal reservoirs induced decoherence through the dissipative and phase-damping processes by analytically solving their respective master equations. In our study, we have explicitly included the terms involving the mean number of thermal photons in the master equation describing the dissipative process. This enabled us to clarify the role of reservoir parameters, including its temperature and frequency. It is demonstrated that under the influence of dissipative thermal reservoir not only the brightness of the sub-Planck structures of cat and compass states reduces but also their *size* and *area* become larger, simultaneously. We have also shown that after the finite evolution-time, the *size* and *area* of the phase-space structures involved remain no longer smaller than the limit set by the Heisenberg's uncertainty principle. The *area* of sub-Planck structures is found to be more sensitive to the dissipative reservoir compared to that of *size* as the former increases quickly with respect to the time-evolution. Moreover, it is demonstrated that in contrast to the dissipative reservoir, the phase-space structures of the cat and compass states persist even in the infinitely-long evolution-time limit under phase-damped reservoir.

Aknowledgements

This work is supported by a grant-in aid (104-2811-M-007-023) from the Ministry of Science and Technology, Taiwan. Authors would like to thank Dr. You-Lin Chuang for useful discussions.

References

[1] Y. Shen, S.M. Assad, N.B. Grosse, Y. Li, M.D. Reid, P.K. Lam, Nonlinear entanglement and its application to generating cat states, Phys. Rev. Lett. 114 (2015) 100403.
[2] B.C. Sanders, Review of entangled coherent states, J. Phys. A: Math. Theor. 45 (2012) 244002.
[3] A. Ourjoumtsev, F. Ferreyrol, R. Tualle-Brouri, P. Grangier, Preparation of non-local superpositions of quasi-classical light states, Nat. Phys. 5 (2009) 189–192.
[4] H. Jeong, M.S. Kim, J. Lee, Quantum-information processing for a coherent superposition state via a mixedentangled coherent channel, Phys. Rev. A 64 (2001) 052308.
[5] L. Braunstein, P. van Loock, Quantum information with continuous variables, Rev. Mod. Phys. 77 (2005) 513.
[6] B. Vlastakis, G. Kirchmair, Z. Leghtas, S.E. Nigg, L. Frunzio, S.M. Girvin, M. Mirrahimi, M.H. Devoret, R.J. Schoelkopf, Deterministically encoding quantum information using 100-photon Schrödinger cat states, Science 342 (2013) 607–610.
[7] W.H. Zurek, Sub-Planck structure in phase space and its relevance for quantum decoherence, Nature 412 (2001) 712–717.
[8] S. Ghosh, R. Sharma, U. Roy, P.K. Panigrahi, Mesoscopic quantum superposition of the generalized cat state: a diffraction limit, Phys. Rev. A 92 (2015) 053819.
[9] L. Praxmeyer, C.-C. Chen, P. Yang, S.-D. Yang, R.-K. Lee, Demonstration of sub-Planck structures from compass states in time-frequency domain, Phys. Rev. A 93 (2016) 053835.
[10] F. Toscano, D.A.R. Dalvit, L. Davidovich, W.H. Zurek, Sub-Planck phase-space structures and Heisenberg-limited measurements, Phys. Rev. A 73 (2006) 023803.
[11] M. Stobińska, G.J. Milburn, K. Wódkiewicz, Wigner function evolution of quantum states in the presence of self-Kerr interaction, Phys. Rev. A 78 (2008) 013810.
[12] M. Rohith, C. Sudheesh, Visualizing revivals and fractional revivals in a Kerr medium using an optical tomogram, Phys. Rev. A 92 (2015) 053828.
[13] S. Ghosh, U. Roy, C. Genes, D. Vitali, Sub-Planck-scale structures in a vibrating molecule in the presence of decoherence, Phys. Rev. A 79 (2009) 052104.
[14] S. Ghosh, A. Chiruvelli, J. Banerji, P.K. Panigrahi, Mesoscopic superposition and sub-Planck-scale structure in molecular wave packets, Phys. Rev. A 73 (2006) 013411.
[15] S. Bose, K. Jacobs, P.L. Knight, Preparation of nonclassical states in cavities with a moving mirror, Phys. Rev. A 56 (1997) 4175.
[16] G.S. Agarwal, P.K. Pathak, Mesoscopic superposition of states with sub-Planck structures in phase space, Phys. Rev. A 70 (2004) 053813.
[17] L. Davidovich, M. Brune, J.M. Raimond, S. Haroche, Mesoscopic quantum coherences in cavity QED: preparation and decoherence monitoring schemes, Phys. Rev. A 53 (1996) 1295.
[18] A. Ghosh, P.K. Das, Generation of a superposition of coherent states in a resonant cavity and its nonclassicality and decoherence, Can. J. Phys. 86 (2008) 811–818.
[19] M.S. Kim, V. Bužek, Schrödinger-cat states at finite temperature: influence of a finite-temperature heat bath on quantum interferences, Phys. Rev. A 46 (1992) 4239.
[20] A. Serafini, M.G.A. Paris, F. Illuminati, S.D. Siena, Quantifying decoherence in continuous variable systems, J. Opt. B. Quantum Semiclass. Opt. 7 (2005) R19.
[21] F. Nicacio, R.N.P. Maia, F. Toscano, R.O. Vallejos, Phase space structure of generalized Gaussian cat states, Phys. Lett. A 374 (2010) 4385–4392.
[22] S. Haroche, J.-M. Raimond, Exploring the Quantum: Atoms, Cavities, and Photons, Oxford University Press, 2006.
[23] C.W. Gardiner, P. Zoller, Quantum Noise, Springer-Verlag, 2004.
[24] A. Biswas, G.S. Agarwal, Nonclassicality and decoherence of photon-subtracted squeezed states, Phys. Rev. A 75 (2007) 032104.
[25] A.-S.F. Obada, H.A. Hessian, A.-B.A. Mohamed, Effect of phase-damped cavity on dynamics of tangles of a nondegenerate two-photon JC model, Opt. Commun. 281 (2008) 5189–5193.
[26] A.-S.F. Obada, H.A. Hessian, A.-B.A. Mohamed, M. Hashem, Effects of a phase-damping cavity on entanglement and purity loss in two-qubit system, Quantum Inf. Process. 14 (2015) 2043–2053.
[27] S. Posen, M. Liepe, Advances in development of Nb_3Sn superconducting radio-frequency cavities, Phys. Rev. ST Accel. Beams 17 (2014) 112001.
[28] C. Becker, S. Posen, N. Groll, R. Cook, C.M. Schlepütz, D.L. Hall, M. Liepe, M. Pellin, J. Zasadzinski, T. Proslier, Analysis of Nb_3Sn surface layers for superconducting radio frequency cavity applications, Appl. Phys. Lett. 106 (2015) 082602.